Available online at www.jrors.ir

Journal Of Radar and Optical Remote Sensing

JRORS 00 (2018) 00–00

Facies Evolutions in the Playa of Hoz-e Soltan

Manijeh Ghahroudi Tali [a*], Khadijeh Alinoori[b]

[a]*Professor, Department of Physical Geography, Faculty of Earth Sciences Shahid BeheshtiUniversity, Iran.*
[b]*postdoctoral researcher, Department of Physical Geography, Faculty of Earth Sciences, Shahid Beheshti University, Iran.*

Received 00 September 2018; revised 00 November 2018; accepted 00 November 2018

Abstract

Hoz-e-Sultan's playa, one of the lowest locations on the Iran plateau, is crucial to the region's climate equilibrium and ecological changes. As a result, studying the deformation and disturbance of facies induced by human interventions and climate change, as well as identifying equilibrium thresholds is critical. In the present research, the amount of deformation and equilibrium thresholds were evaluated over five years, using ASAR C-band radar images and the differential interferometry technique from 2004 to 2009.Comparing the results of radar images and playa facies in a short—and medium-term temporal scale showed that the facies disturbances were increased, and dynamic equilibrium was changed. Therefore, the total changes that occurred during 2004-2009 were -3.4, with the direction of non-equilibrium (negative) in the muddy facies in the north and (positive) 5.3 in the clay facies in the west of the region. Playa had the most non-equilibrium during 2004-2005 and 2007-2008, while it had more stable conditions during 2004-2006 and 2008-2009. During 2004-2009, southern playa was in a relative equilibrium. The non-equilibrium range occasionally extends towards the north of the playa, and it has progressed on the facies of the northwestern boundary because of increased human interference.

Keywords: playa**,** facies, equilibrium, Envisat

* Corresponding author. Tel:.+989121263968
E-mail address: m-ghahroudi@sbu.ac.ir

1. Introduction

Many potential dangers, ground non-equilibrium, and stability, as well as many theories and concepts of geomorphology, require the use of radar data and differential interferometric processing methods. In monitoring landslides and estimating their displacement, it can demonstrate the activity of the landslide masses. In recent years, the analysis of ENVISAT radar images in sliding masses recorded in 2011 revealed a time interval of 150 days equal to 8 cm and a time interval of 4 years equivalent to 28.8 cm in the railway territory of Lorestan railway (Shirani and Khoshbatan 2016; Afshari et al. 2019). Radar satellite images have also been used to study the subsidence of numerous Iranian plains. In the plains of Tehran, Karaj, Shahriyar, Sabzevar, Moghan, and Rafsanjan, the total yearly subsidence is more than 60 cm each year (Chatar Simab et al. 2020; Ghahroudi et al. 2021; Sharifi Kia et al. 2015; Hassan Shahi and Sarkargar Ardakani, 2019). Using ENVISAT satellite data from the study period of 2004-2009, this phenomenon was observed in the highly significant ancient regions of Persepolis, Hoz, Naghsh-e Rostam, and Naghsh-e-Rajab (Daneshmandi, 2018). The volume of rockfall and its position can be observed using radar satellites and differential interferometry methods. Karimi and Al-Modarresi (2019), for example, used 12 images from 2016 and three pebbles from 2014 and 2015 to investigate the number of rockfalls on Haraz Road.

Piri et al. (2018) and Farzin Kia et al. (2019) introduced the notion of geo-duality utilizing radar interferometry to verify novel geomorphological concepts and theories. Sustainability is an essential idea in earth sciences, and its application can be seen in various areas. Roustaei et al. (2016) used ENVISAT satellite radar images and the radar differential interferometry (D-INSAR) technique to determine the optimal location and evaluate the stability of the chosen location for the displacement of the Gugerd village. They found that the selected location is unstable and has an average displacement of 12 cm per year. In addition, radar images from the Sentinel 1 satellite were utilized to locate and calculate the velocity of materials on unstable slopes facing railway lines in the Lorestan area during 2015-2018. Its volume was estimated to be 28.8 cm, indicating that the slope motion is active in the area (Afshari et al. 2019). The degree of stability is affected by its deformation and velocity. Synthetic aperture radar time series is a method for measuring land deformation that can track deformation over a vast region. Its effectiveness in investigating various land deformation processes has been well established. Recognizing and comprehending the deformation of phenomena requires noise assessment and the investigation of temporal and spatial correlation of deformation series derived by radar interferometry (Tahmasebi et al. 2015). Stramondo et al. (2005) evaluated the deformation produced by the Bam earthquake in southwestern Iran using ENVISAT C-band (ASAR) images taken on December 26, 2003. In addition, Jafari et al. (2015) studied the deformation caused by the 5.7 earthquake magnitude that struck near Ghatour of Khoy city in West Azerbaijan province on February 23, 2020. SAR (DInSAR) was employed to examine surface deformation at two different spatial scales: low resolution-large scale, and high resolution-local scale (Moghaddam et al. 2011; Monta et al. 2008). They investigated the signs of surface deformation caused by the evacuation of hydrocarbon fluid by studying many production sites in a time series of view interference during 2003-2008. The connection of deformation to man-made structures (over 15 years) was shown by examining ERS and ENVISAT datasets related to the Gulf of Naples and Morges, and the mean velocity map of Hashtgerd plain in 2008 revealed a rate of 47 mm per month (Manuela et al. 2012; Haghighat Mehr et al. 2012). Tahmasebi et al. (2015) used the radar interferometry method to achieve a time series of subsidence-induced deformation in the Mahyar Plain area in Isfahan province. In addition, Mehrnoosh Ghadimi and Ali Derakhshan (2020) used 1A-Sentinel images to study the deformation in Taleghan Dam from 2014 to 2019. These images were also used to investigate areas with significant spatial and temporal deformation gradients. Due to the lack of integrated monitoring and forecasting models for closed mines and the unclear spatio-temporal development model of closed surface deformation, the SBAS InSAR technology and 1A-Sentinel images were employed (Chen et al. 2022). Choupani et al. (2020) used interferometric synthetic aperture radar (SBAS-InSAR) to study the deformation during 2004-2010. The identical images of deformation curves were first exposed in detail in

the ever-frozen Gladandong area, the Tangola Mountains on the Tibetan Plateau, during 2017-2020 (Wang et al. 2022).

Several interactions occur on small to big dimensions in arid and semi-arid conditions (Sako et al. 2007). Monitoring such patterning in dry conditions offers a unique opportunity to comprehend landscape processes (Petrasiac et al. 2014). Nevertheless, the playas in the confined basin get their water mostly from direct rainfall and runoff at the lowest elevations (Hawks and Smith 1994; Thiner 2003). There is no natural outlet for them. A set of unique soils known as hydrogen soils frequently characterize these places (Rosen 1994; Smith 2003; Schatzel and Anderson, 2005). The wealth of old environmental knowledge is preserved by playa deposits (Sepehr et al. 2013). Since prehistoric times, playas have had a profound effect on human communities as water and mineral resources. They are now utilized in urban development (Cook et al. 1982). Climate change and human involvement have caused considerable changes in groundwater flows, disturbing the playas' equilibrium. Substantial and relatively brief changes in hydrological equilibrium and sedimentation have resulted in important, pervasive, and frequently unfavorable environmental consequences (Paul and Bryant 2011; Gill 1996). Their harmful influence is now acknowledged as a significant producer of atmospheric dust (Bridge and Demico 2008).Considering what was mentioned above, the condition of stability and equilibrium is critical in a cognitive system since disturbing the equilibrium between the many elements of the basin affects its stability. Therefore, to be able to manage the evolution of a system, the stability state thresholds of a system should be well understood (Ramesht and Shahzidi 2011). As previously said, human interventions force the natural environment to the point of non-equilibrium, and intentional interventions are required to bring the environment to a state where it can somehow recover its equilibrium. Therefore, it is necessary to predict unexpected environmental changes and make optimal use of resources. The Playa's natural environment is crucial in predicting these abrupt changes. Lack of acquaintance with it leads to a lack of understanding of numerous natural environment facts, which can be regarded as a vacuum in one of the aspects of planning and risk management knowledge (Ghahroudi Tali and Alinoori, 2015). Consequently, these connections should be investigated before human intervention becomes widespread. The timely availability of fresh information will aid future decision-making and develop these fragile and sensitive regions (Jung et al. 2004). Meanwhile, these efforts have affected Houz-e Sultan's Playa. Hence its equilibrium thresholds have been altered. Since radar images and radar interferometry techniques are essential in the research of stability and equilibrium, the playa facies considering the spatial model of their distribution, and the deformations induced by these interventions, as well as the amount of resulting non-equilibrium have been analyzed using ENVISAT-ASAR images with radar differential interferometry technique.

2. Materials and methods

2.1. The Study Area

Houz-e Sultan Playa, located 85 kilometers southwest of Tehran and covering 104.4 km2, has a catchment area of roughly 195 square kilometers. In addition, it is situatedbetween 50° 68′ to 50° 50 ′ eastern longitude and 34° 74′ to 35° 17′ northern latitude of the equator (Figure 1) (Shafiei Darabi et al. 2013).

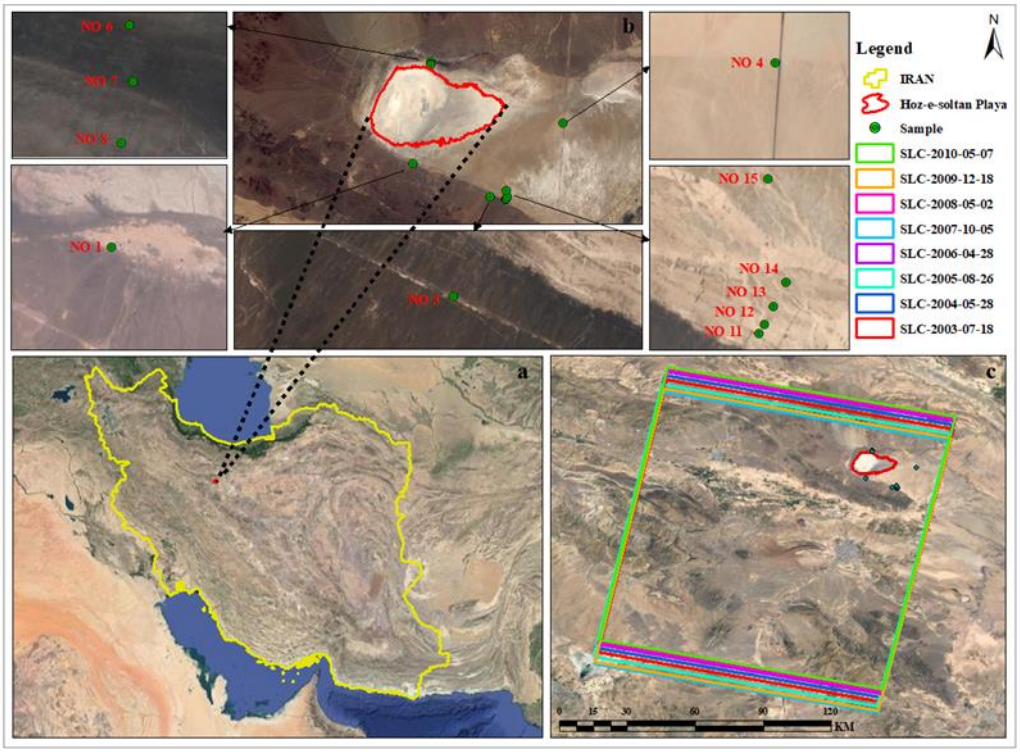

Figure 1. a (Location of Iran (b) Location of Hoz-e-Sultan playa and sampling stations, C) Study area and SLC border of ENVISAT ASAR images during 2003-2010 on google Satellite images.

2.2. Data

The present research used ground data, satellite data, and information gathered during the initial processing step of radar images. The researchers used field surveys to collect ground data (Table 1). The European Space Agency contributed satellite data (Table 2). Table 3. shows data derived from the analysis of satellite data.

Table 1. The location and height of sampling points in the Hoz-e Sultan Playa

Sample code	x	y	Sample height (m)
NO1	50.9463	34.9334	803
NO3	51.0495	34.8973	817
NO4	51.1459	34.9778	807.6
NO6	50.9711	35.0439	799.7
NO7	50.9712	35.0424	798.6
NO8	50.9709	35.0408	797.6
NO11	51.0697	34.8942	812.5
NO12	51.0701	34.8948	812.5
NO13	51.0708	34.8960	812.2
NO14	51.0718	34.8976	810.9
NO15	51.0704	34.9045	809

Table 2. The specifications of the radar images

MISSION	SENSOR	date	SWATH	Track	Frame	Orbit	Polarisation	Pass	Start time	Stop time
Envisat-1	ASAR/IM	2003-07-18	12	149	2907	7217	descending	VV	6:48:46.7	6:49:01.56
Envisat-1	ASAR/IM	2004-05-28	12	149	2907	11726	descending	VV	6:48:49.15	6:49:04.24

Envisat-1	ASAR/IM	2005-08-26	12	149	2907	18239	descending	VV	6:48:47.66	6:49:02.75
Envisat-1	ASAR/IM	2006-04-28	12	149	2907	21746	descending	VV	6:48:41.03	6:48:56.12
Envisat-1	ASAR/IM	2007-10-05	12	149	2907	29261	descending	VV	6:48:39.66	6:48:54.75
Envisat-1	ASAR/IM	2008-05-02	12	149	2907	32267	descending	VV	6:48:36.11	6:48:51.20
Envisat-1	ASAR/IM	2009-12-18	12	149	2907	40784	descending	VV	6:48:29.74	6:48:44.83
Envisat-1	ASAR/IM	2010-05-07	12	149	2907	42788	descending	VV	6:48:26.89	6:48:41.98

Table 3. The specifications of processed interferograms in the study area

Spatial Base line (meter)	ambiguity height	Master	Slave	interferogram
866.712	10.632	2003/07/18	2004/05/28	a
71.469	128.957	2004/05/28	2005/08/26	b
325.810	28.291	2005/08/26	2006/04/28	c
370.629	24.461	2006/04/28	2007/10/05	d
39.437	233.618	2007/10/05	2008/05/02	e
158.358	58.213	2008/05/02	2009/12/18	f
468.895	19.656	2009/12/18	2010/05/07	g
577.153	15.967	2003/07/18	2010/05/07	h

2.3. Radar differential interferometry technique

- The researchers used radar differential interferometry techniques to depict facies alterations and analyze short- and long-term temporal variations. The ENVISAT satellite ASAR sensor provided 8 C-band SLC images utilized in this investigation. The European Space Agency (ESA) provided these images from 2003-2010 with a wavelength of 5.6 cm for April, May, July, August, October, and December. The study used SARSCAPE software to process radar images of Houz-e Soltan Playa during the main steps as follows:Converting images to standard Sarscape format: The DOR - VOR file, which comprises data gathered by the European Space Agency's DORIS satellite, was used to rectify image distortion via orbital information processing.
- Conformity of two SLC images: The interference measurement baseline was determined at this point, and the images were validated for spatial baseline.
- To obtain the amount of surface displacement, all other effects were eliminated from the interferograms. The elevation model (SRTM DEM) with a spatial resolution of 90 meters was used to reduce the majority of the topographical influence in producing the phase difference of the images.
- The adaptive filter was used to reduce eight interferogram noises from the previous stage(Figure 2).
- The phase opening: The synthetic phases were merged with the absolute calibration phase and the opened phases to create a height and coded map. The coherence image was also encoded as a result of this stage. After that, two files were created by encoding the digital elevation model and the coherence image: the velocity file, which is derived from parameters such as coherence,base, and wavelength; and the resolution file, which depicts the ground's pixel resolution (Equation 1) (Holkes et al. 1997).

: 1 Equation

$$\frac{pixel\ distance\ slope\ area}{\sin(loal\ collusion\ angle)}$$

- · The procedure of adjusting and re-leveling the interferogram used the stage of producing a ground control point as an input.
- · The correction and leveling procedure was repeated on the images.

- · Phase conversion image stage: The phase values were converted to displacement and then coded on a map to produce a displacement map.

· The image in the study area was zoned during 2004-2009, and the number of changes was determined.

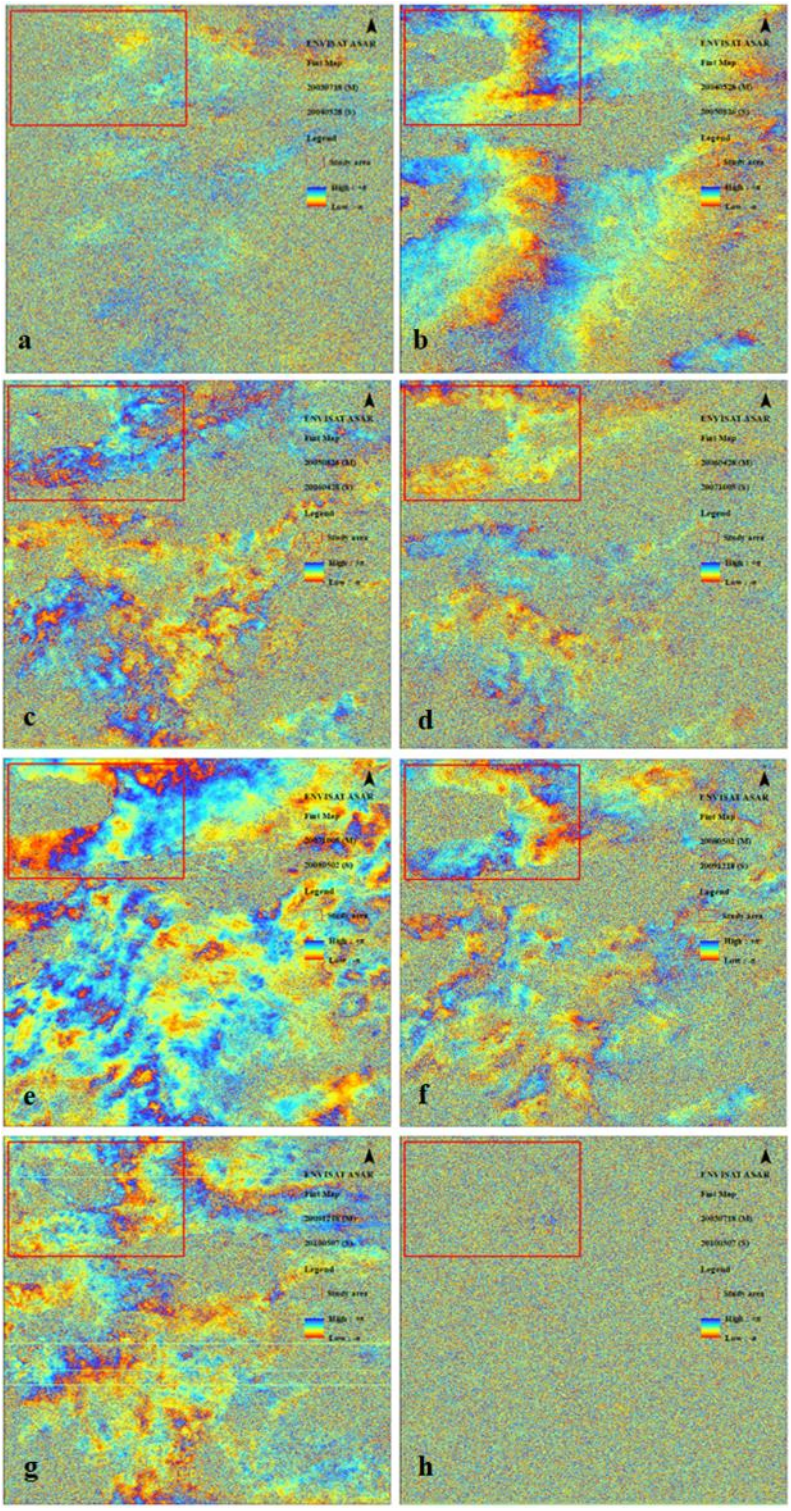

Figure 2. The interferogram processed with an Adaptive filter for 2003-2010, which are as follows: The interferogram related to 18/07/2003- 28/05/2004 (314 days), b) The interferogram related to 28/05/2004- 26/08/2005 (524 days), c) The interferogram related to 26/08/2005- 28/04/2006 (246 days), d) The interferogram related to 28/04/2006- 05/10/2007 (526 days), e) The interferogram related to 05/10/2007- 02/05/2008 (210 days), f) The interferogram related to 02/05/2008- 18/12/2009 (596 days), g) The interferogram related to 18/12/2009- 07/05/2010 (141 days), h) The interferogram related to 18/07/2003- 07/05/2010 (141 days)

2.4. Field studies

Field surveys were conducted in the wet, sulfate, and carbonate zones of the Hoz-e Soltan's Playa in May to evaluate the equilibrium changes of the facies (May 2014, June and August 2016). The field visit comprised a review of the Playa's condition, physical features, and specimen photography. Table 1 indicates the position and height of the sampling points (1). Figure 3 shows the facies examined in Playa.

Figure 3. The studied facies of Hoz-e Soltan's Playa: a) Muddy cracks in the mud-clay facies, b) Salty nodules in muddy-salty facies c) Puffy clay in muddy-salty clay facies, d) Colloform mud in muddy-salty facies, e) Clay polygon in muddy-clay facies, f) Puffy salt crack in muddy-clay facies, g) muddy-puffy cracks in the muddy clay facies, h) Salty polygon in salty facies, i) Clay cracks in clay facies, j) muddy-puffy polygon in salty-clay facies, k) muddy-salty polygon in muddy-salty facies

2.5. Research flow chart

ENVI software and the phase interferometry SARSCAPE adjoint software were used to implement the radar differential interferometry technique. Changes occurring at the ground level over two periods were analyzed from similar locations using radar phase information and ground reflections. The assessment of ground surface changes involved evaluating and modeling the phase difference. Field sampling and facies separation were done, and then the changes in the Playa facies were measured in millimeters by overlaying the samples with deformation images. Figure (4) depicts the steps taken in the research.

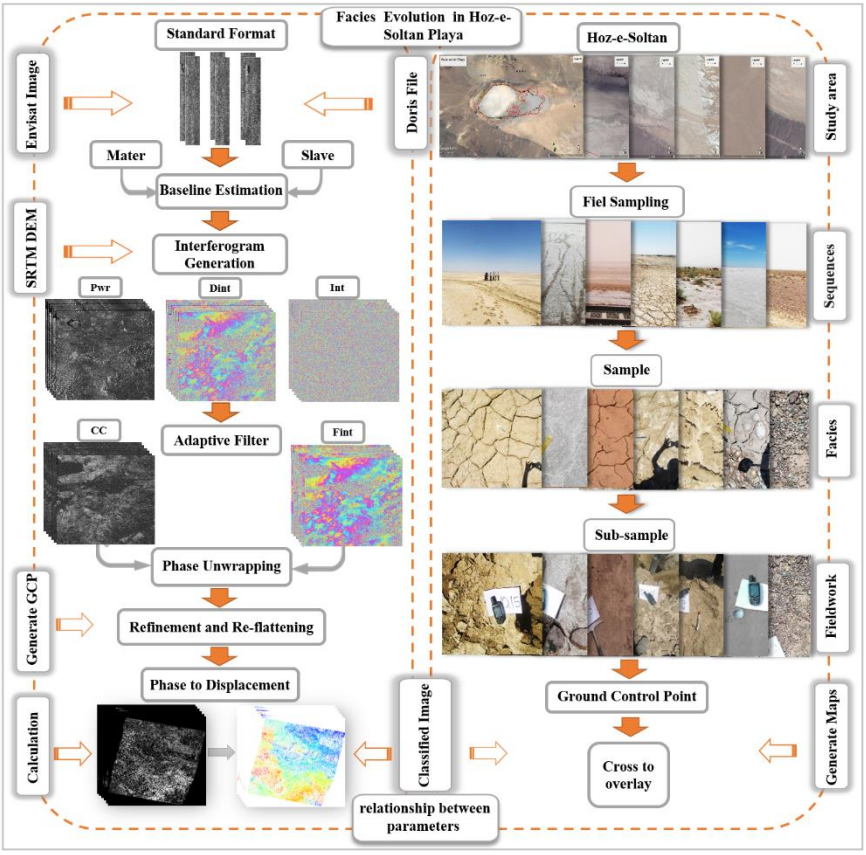

Figure 4. The research flow chart in the Hoz-e Soltan's Playa.

3. Results and Discussion

The researchers divided the generated interferograms into two groups, one with a time interval of less than one year and the other with more than one year. The images' coherence was assessed to find interferograms with a high degree of coherence for deformation analysis. The coherence images were studied during 2003-2010 (Figure 5). The coherence rates during the periods of July 18, 2003, to May 28, 2004; April 28, 2006, to May 10, 2007; and July 18, 2003, to May 7, 2010, fell within a histogram range of 0.2 to 0.4, with time intervals of 314, 526, and 2632 days, respectively. These interferograms, on the other hand, show a lower degree of coherence compared to other pairs of images, according to their spatial baseline (Table 4). The coherence rate of the interferogram during the period from December 18, 2009, to July 5, 2010, with an interval of 141 days, achieved its highest level within the coherence range of 0.6 to 0.2 (measured in pixel frequency). However, compared to processed interferograms, it has an average coherence rate due to its high spatial baseline of 468/895. Interferograms for 2004-2005, 2005-2006, 2007-2008, and 2008-2009 had relatively less spatial baseline compared to other interferograms concerning the temporal baseline during 2003-2010 among the eight interferograms extracted in this study at the intervals of less than one year and more than one year, showing less non-correlation caused by phase noise. Because these images have a higher degree of coherence than other interferograms, the researchers selected them to investigate and assess the extent of deformation and changes in the area.

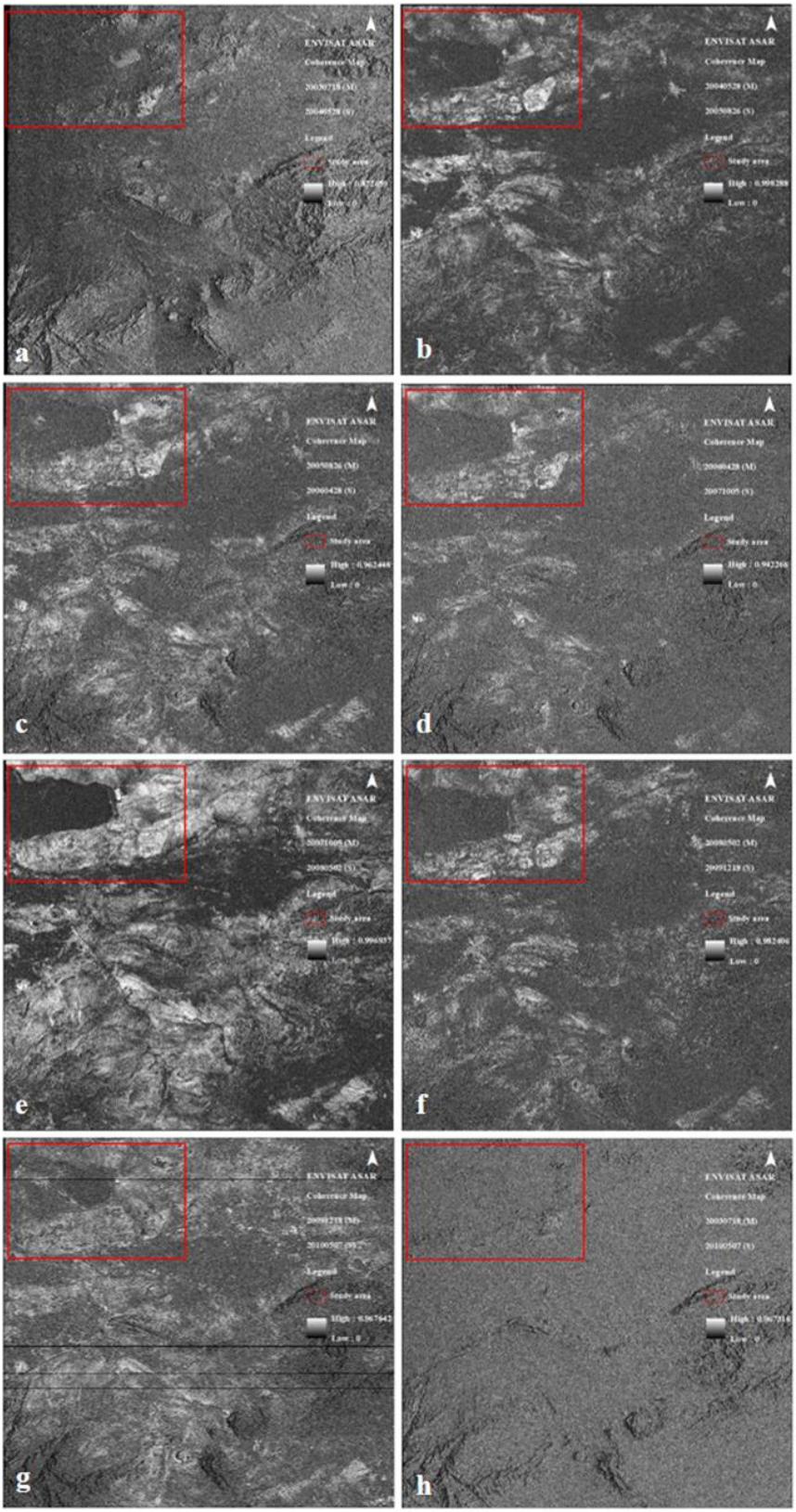

Figure 5. The coherence image related to 2004-2010 of Houz-e Sultan's playa

Table 4. The statistical information of images in terms of coherence

The highest frequency of	Distribution of coherence values of the	Spatial baseline (m)	Temporal baseline (days)	Standard deviation	Mean	Minimum	Maximum	Coherence images of the time interval2004-2010
0.2-0.4	0-0.4	866.712	314	0.069	0.16	0	0.955	2003/07/18-2004/05/28
0.2-0.4	0-0.6	71.469	452	0.116	0.255	0	0.998	2004/05/28-2005/08/26
0.2-0.4	0.2-0.6	325.81	246	0.112	0.253	0	0.98	2005/08/26-2006/04/28
0.2-0.4	0.2-0.4	370.629	526	0.103	0.228	0	0.977	2006/04/28-2007/10/05
0.2-0.6	0.2-0.8	39.437	210	0.172	0.312	0	0.999	2007/10/05-2008/05/02
0.2-0.4	0.2-0.4	158.358	596	0.112	0.231	0	0.993	2008/05/02-2009/12/18
0.2-0.4	0.2-0.6	468.895	141	0.124	0.248	0	0.979	2009/12/18-2010/05/07
0.2-0.4	0-0.4	577.153	2632	0.083	0.208	0	0.985	2003/07/18-2010/05/07

3.1. Deformation analysis of DInSAR

A statistical analysis found that out of four interferograms, two have a period of less than one year, and two have a period of more than one year. They will be interpreted below. 3.1.1. Studying the DInSAR deformation in less than one year

The minimum temporal baseline is established from Slave and Master images from the periods 26/08/2005-28/04/2006 and 05/10/2007-02/05/2008, respectively, with the time intervals of 246 and 210 days. Since the time gap was less than a year, a few distortion was expected in the overlap between the two images. The created deformation map, however, revealed that several of the zones were non-equilibrium. The deformations in the facies intervention during 2005-2006 fluctuated between -6 and 6.8. As shown in Figure 6, the center area and, to a lesser extent, the north area has experienced rapid transformation. The samples gathered from various facies of the Houz-e Sultan playa throughout the playa zones revealed that samples No. 4, No.12, No.13, and No.14 with clay facies (mm6), salty-muddy facies (mm2), muddy-salty facies (mm5), and muddy-salty facies (mm2) have been in a negative non-equilibrium state, respectively. The samples No.6 and No.11 have been in the salty-muddy facies (mm6) and clay-muddy facies (mm1) in a positive non-equilibrium state, respectively (Figure 5). Stable zones are located around the research area, particularly around the margins of unstable areas surrounding the unstable centers.

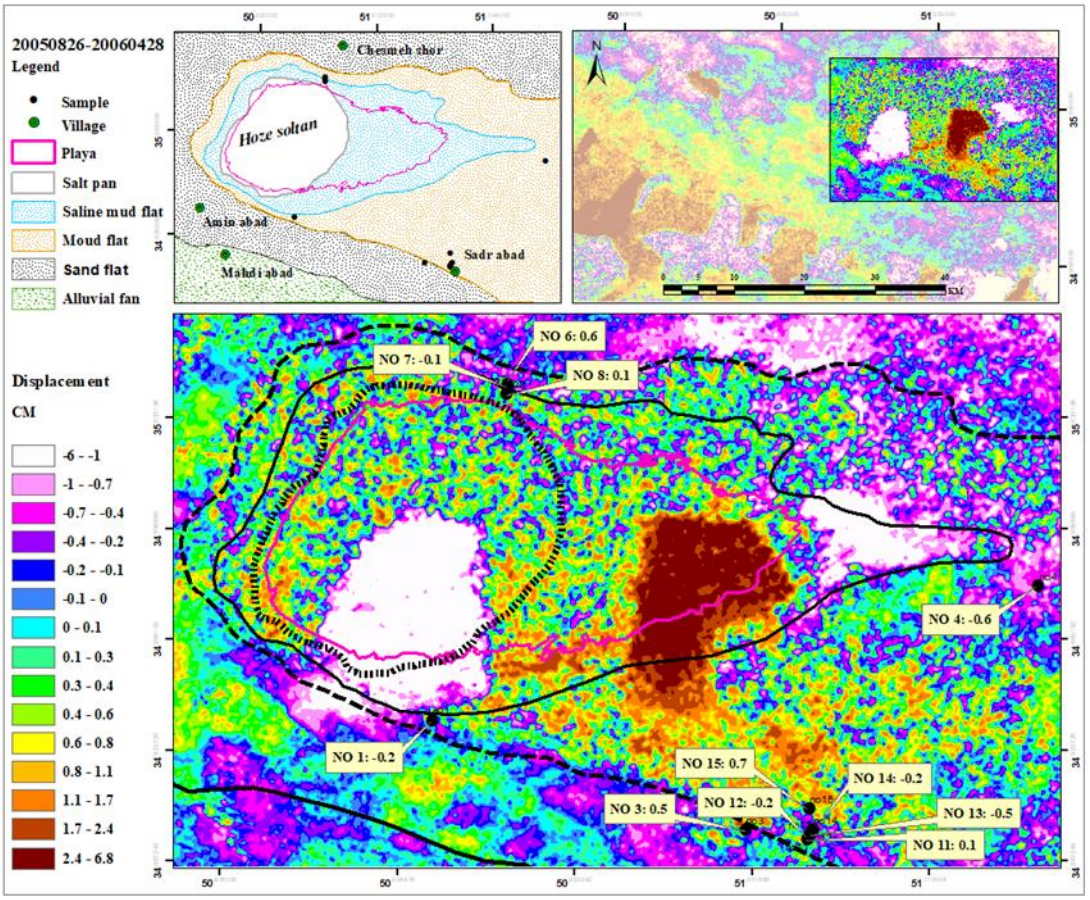

Figure 6. Zoning of facies deformation in the playa on the displacement image during 26/08/2005-28/04/2006.

Table 5. The facies developments during 26/08/2005-04/28/2006 in the studied area

Period 26/08/2005-28/04/2006					
Sample code	Zone	Facies	Changes direction	Value per cm	Equilibrium status
NO1	Muddy zone	Clay-muddy	↓	-0.2	Negative non-equilibrium
NO3	Sandy zone	Muddy-clay	↑	0.5	Positive non-equilibrium
NO4	Muddy zone	Clay	↓	-0.6	Negative non-equilibrium
NO6	Muddy zone	Muddy-salty	↑	0.6	Positive non-equilibrium
NO7	Muddy-salty zone	Salty-muddy	↓	-0.1	Negative non-equilibrium
NO8	Muddy-salty zone	Salty	↑	0.1	Positive non-equilibrium
NO11	Muddy zone	Clay-muddy	↑	0.1	Positive non-equilibrium
NO12	Muddy zone	Salty-muddy	↓	-0.2	Negative non-equilibrium
NO13	Muddy zone	Salty-muddy	↓	-0.5	Negative non-equilibrium
NO14	Muddy zone	Muddy-salty	↓	-0.2	Negative non-equilibrium
NO15	Muddy zone	Salty-clay-muddy	↑	0.7	Positive non-equilibrium

As demonstrated in Figure 7, the maximum negative change recorded was -0.9 cm in Playa and its central parts, while the minimum change was in the sandy zones of Playa's southern, southwestern, and western areas. The research area has become more sustainable from north to south of Playa. Positive developments toward non-equilibrium have begun in the southwest. Based on samples obtained from different facies of the Hoz-e-Soltan Playa during this period, the muddy-salty facies had the maximum changes in the direction of negative non-equilibrium with 3.4 cm, while the clay-muddy facies is in a sustainable state (Table 6).

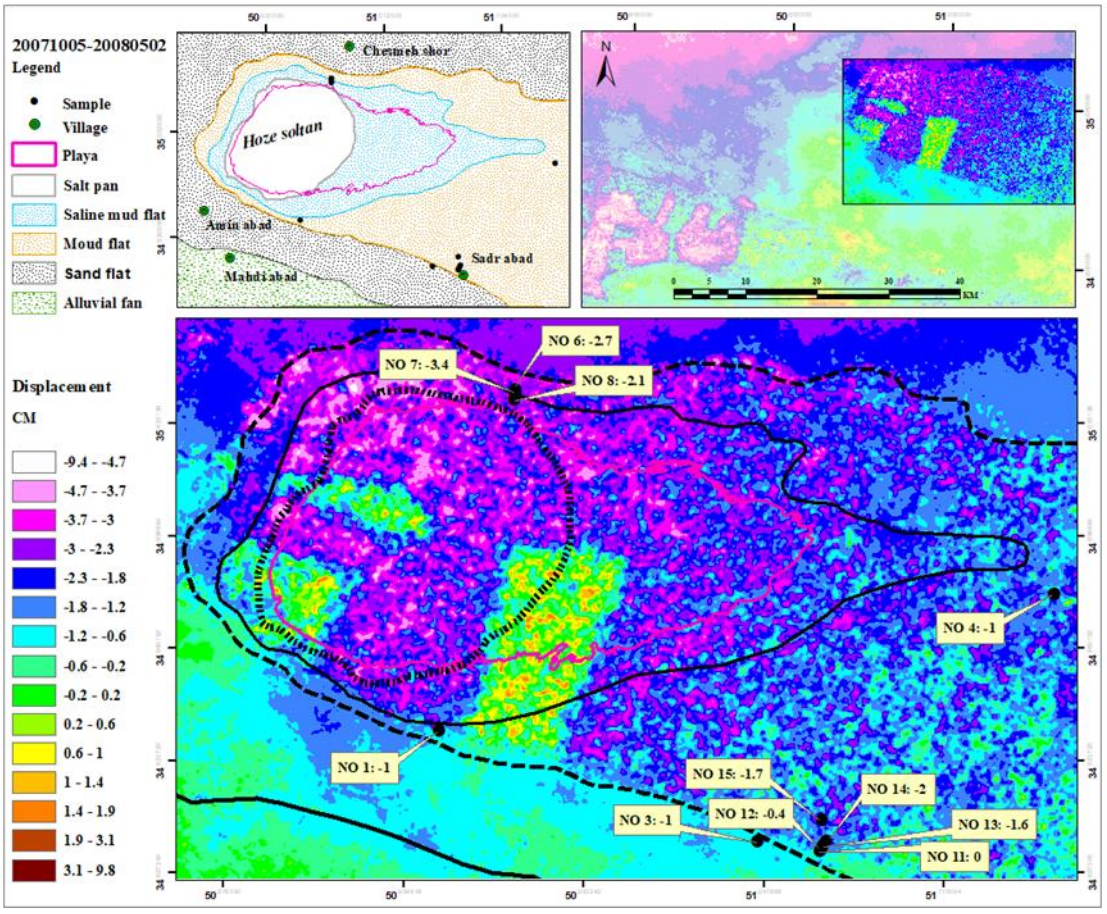

Figure 7. Zoning of facies deformation in the playa on the displacement image during 26/08/2005-28/04/2006

Table 6. The facies developments during 26/08/2005-04/28/2006 in the studied area

Period 26/08/2005-28/04/2006					
Sample code	Zone	Facies	Changes direction	Value per cm	Equilibrium status
NO1	Muddy zone	Clay-muddy	↓	-1	Negative non-equilibrium
NO3	Sandy zone	Muddy-clay	↓	-1	Negative non-equilibrium
NO4	Muddy zone	Clay	↓	-1	Negative non-equilibrium
NO6	Muddy zone	Muddy-salty	↑	-2.7	Negative non-equilibrium
NO7	Muddy-salty zone	Salty-muddy	↓	-3.4	Negative non-equilibrium
NO8	Muddy-salty zone	Salty	↓	-2.1	Negative non-equilibrium
NO11	Muddy zone	Clay-muddy	↕	0	Sustainable
NO12	Muddy zone	Salty-muddy	↓	-0.4	Negative non-equilibrium
NO13	Muddy zone	Salty-muddy	↓	-1.6	Negative non-equilibrium
NO14	Muddy zone	Muddy-salty	↓	-2	Negative non-equilibrium
NO15	Muddy zone	Salty-clay-muddy	↓	-1.7	Negative non-equilibrium

3.1.2. Studying DInSAR Deformation in More Than One Year

The maximum temporal baseline is observed in slave and master images from 28/05/2004-26/08/2005 and -02/05/2008-07/12/2009, respectively, with intervals of 452 and 596 days. The created deformation map revealed that all study regions, except the western region, were in a positive non-equilibrium state, with the highest value associated with clay facies sample no. 4. (5.3 cm). In sample no1, the negative non-equilibrium reaches the quantity (mm2) in the clay facies. These changes reflect the region's rapid rate of development over such a short period (Figure 8, Table 7). According to surveys, most alterations occurred in the northeastern portion of Playa between 2008 and 2009. The southeastern portions of Playa are reasonably stable, with fluctuations owing to non-equilibrium steadily decreasing to the southeast. Considering the samples obtained from different facies of the Hoz-e-Soltan Playa at this time, sample No. 8 of salty facies (1.9 cm) exhibited the most changes toward negative non-equilibrium. However, sample No. 3 of clay facies remained constant. Furthermore, the highest positive non-equilibrium values were found in muddy and muddy-salty facies in samples no11 and no15 (7 mm) (Figure 9, Table 8).

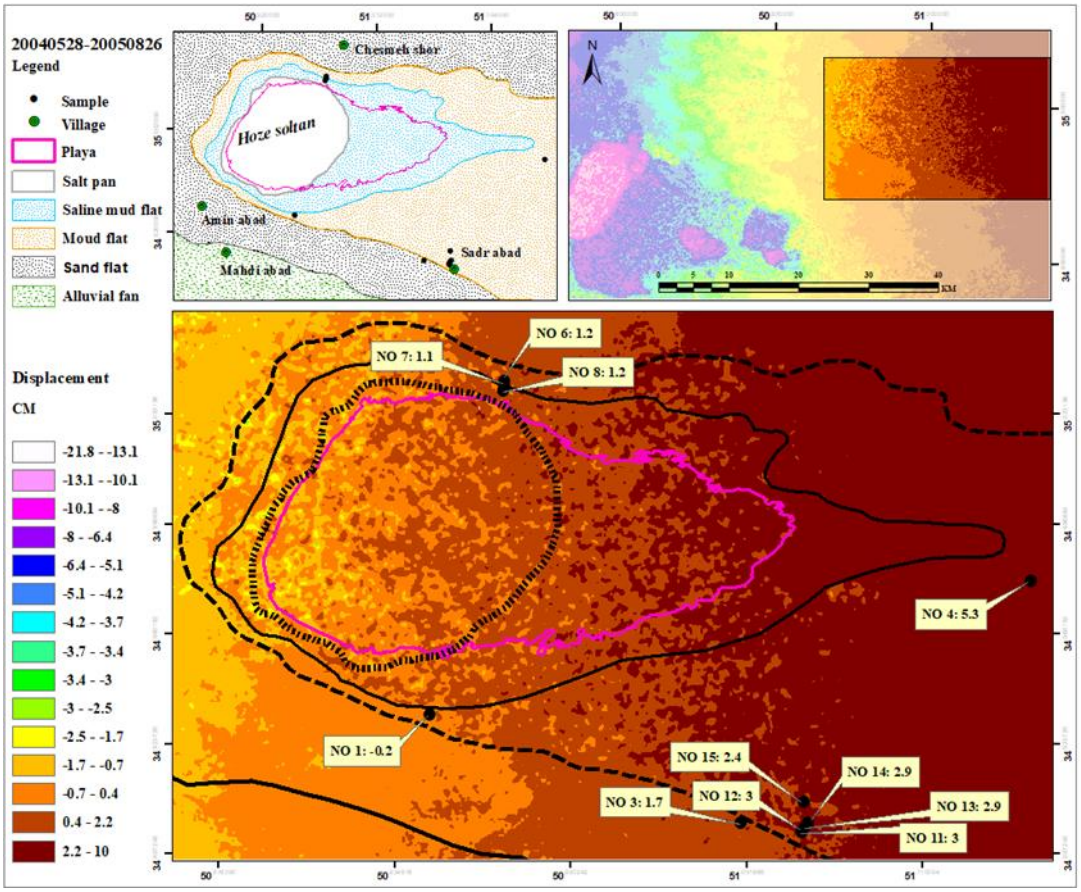

Figure 8. Zoning of facies deformation in the playa on the displacement image during 26/08/2005-28/04/2006

Table 7. The facies developments during 26/08/2005-04/28/2006 in the studied area

Period 26/08/2005-28/04/2006					
Sample code	Zone	Facies	Changes direction	Value per cm	Equilibrium status
NO1	Muddy zone	Clay-muddy	↓	-0.2	Negative non-equilibrium
NO3	Sandy zone	Muddy-clay	↑	1.7	Positive non-equilibrium
NO4	Muddy zone	Clay	↑	5.3	Positive non-equilibrium
NO6	Muddy zone	Muddy-salty	↑	1.2	Positive non-equilibrium
NO7	Muddy-salty zone	Salty-muddy	↑	1.1	Positive non-equilibrium
NO8	Muddy-salty zone	Salty	↑	1.2	Positive non-equilibrium
NO11	Muddy zone	Clay-muddy	↑	3	Positive non-equilibrium
NO12	Muddy zone	Salty-muddy	↑	3	Positive non-equilibrium
NO13	Muddy zone	Salty-muddy	↑	2.9	Positive non-equilibrium
NO14	Muddy zone	Muddy-salty	↑	2.9	Positive non-equilibrium
NO15	Muddy zone	Salty-clay-muddy	↑	2.4	Positive non-equilibrium

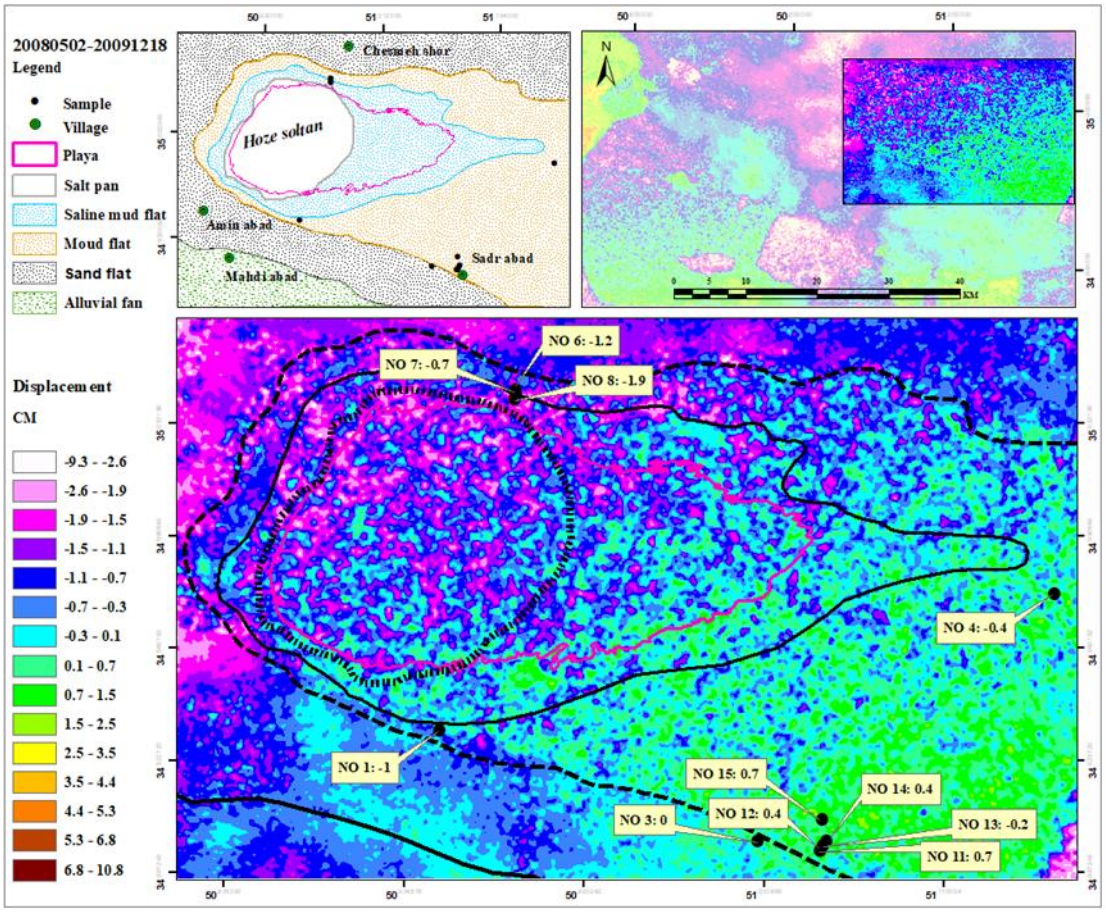

Figure 9. Zoning of facies deformation in the playa on the displacement image during 26/08/2005-28/04/2006

Table 8. The facies developments during 26/08/2005-04/28/2006 in the studied area

Period 26/08/2005-28/04/2006					
Sample code	Zone	Facies	Changes direction	Value per cm	Equilibrium status
NO1	Muddy zone	Clay-muddy	↓	-1	Negative non-equilibrium
NO3	Sandy zone	Muddy-clay	↑	0	Sustainable
NO4	Muddy zone	Clay	↑	-0.4	Negative non-equilibrium
NO6	Muddy zone	Muddy-salty	↑	-1.2	Negative non-equilibrium
NO7	Muddy-salty zone	Salty-muddy	↑	-0.7	Negative non-equilibrium
NO8	Muddy-salty zone	Salty	↑	-1.9	Negative non-equilibrium
NO11	Muddy zone	Clay-muddy	↑	0.7	Positive non-equilibrium
NO12	Muddy zone	Salty-muddy	↑	0.4	Positive non-equilibrium
NO13	Muddy zone	Salty-muddy	↑	-0.2	Negative non-equilibrium
NO14	Muddy zone	Muddy-salty	↑	0.4	Positive non-equilibrium
NO15	Muddy zone	Salty-clay-muddy	↑	0.7	Positive non-equilibrium

4. Conclusions

Based on the findings, the researchers eliminated the displacement images for 2003-2004, 2010-2003, 2006-2020, and 2009-2010. Then they entered four interferograms with high accuracy and coherence into the stage of interpreting the results to evaluate and compare them with the data acquired. In each image pair, the total facies changes in four interferograms from 2004 to 2009 showed the maximum non-equilibrium of 3.4 cm in a negative direction in the north and 3.5 cm in a positive direction in the west of the region (Table 9).

Table 9. The maximum facies changes rate in all 4 interferograms during 2004-2009

Timespan	Maximum negative non-equilibrium			Maximum positive non-equilibrium		
	Sample	Facies	Value	Sample	Facies	value
2004/05/28-2005/08/26	No1	Clay-muddy	-0.2	No4	Clay	5.3
2005/08/26-2006/04/28	No4	Clay	-0.6	No15	Salty-clay-muddy	0.7
2007/10/05-2008/05/02	No7	Salty-muddy	-3.4	-	-	-
2008/05/02-2009/12/18	No6	Salty	-1.9	No11-15	Salty-clay-muddy	0.7

The clay-muddy facies (No. 11) in 2007-2008 and muddy-clay (NO. 3) in 2008-2009 did not alter and were stable. The findings of maximum changes in the samples also corroborated the results of even images from 2004 to 2009, indicating that the playa facies with the highest changes were No. 4 and No.7. The salty-muddy facies (No.7) had the highest change in the negative direction during the entire sample, whereas the clay-muddy facies (No.1fa1) had the most change in the positive direction. The muddy-salty facies (No.13) in the southeast of Playa experienced the least modifications, according to the mean of facies changes (Table 10).

Table 10. The facies developments during 2004 to 2009 in the studied area

Sample	Facies	The maximum rate of change in the negative direction (cm)	The maximum rate of change in the positive direction (cm)	Mean changes
NO1	Clay-muddy	-1	-	-0.6
NO3	Muddy-clay	-1	1.7	0.3
NO4	Clay	-1	5.3	0.8
NO6	Salty-muddy	-2.7	1.2	-0.5
NO7	Salty-muddy	-3.4	1.1	-3.1
NO8	Salty	-2.1	1.2	-2.7
NO11	Clay-muddy	-	3	0.9
NO12	Salty-muddy	-0.4	3	0.7
NO13	Salty-muddy	-1.6	2.9	0.1
NO14	Muddy-salty	-2	2.9	0.2
NO15	Salty-clay-muddy	-1.7	2.4	0.5

The findings revealed that the study periods of 2004-2005 and 2007-2008 displayed the highest levels of non-equilibrium, whereas the study periods of 2004-2006 and 2008-2009 indicated more stable conditions. Acknowledgements

This study is based on a postdoctoral research project at Shahid Beheshti University, funded by the Iran National Science Foundation (INSF) under contract number 98018289. The European Space Agency provides ENVISAT satellite picture data (ESSA).

References

Afshari, A., Ghahroudi Tali, M., Sadough, H., Ehteshami Moin abadi, M. (2020). Assessment slope instability around Lorestan railway by using differential synthetic aperture radar interferometry (DInSAR). Quantitative Geomorphological Research, 8(3), 183-202.

Chatrsimab, Z., Alesheikh, A., Voosoghi, B., Behzadi, S., Modiri, M. (2021). Investigating the effect of aquifer type and groundwater level drop on subsidence rate using radar interference technique and field data (Case study: Tehran-Karaj-Shahriar aquifer area). Advanced Applied Geology, 10(4), 683-689. doi: 10.22055/aag.2020.30557.2028

Chen, Bingqian, Hao Yu, Xiang Zhang, Zhenhong Li, Jianrong Kang, Yang Yu, Jiale Yang, and Lu Qin. 2022. "Time-Varying Surface Deformation Retrieval and Prediction in Closed Mines through Integration of SBAS InSAR Measurements and LSTM Algorithm" Remote Sensing 14, no. 3: 788. https://doi.org/10.3390/rs14030788

Choopani Atefe, Maryam Dehghani & Mohammad Reza Nikoo (2020) Determining hydrogeological parameters of an aquifer in Sirjan Basin using Envisat ASAR interferometry and groundwater modelling, International Journal of Remote Sensing, 41:2, 655-682, DOI: 10.1080/01431161.2019.1646938.

Daneshmandi Asghar (2018) Geotectonic Critical Analysis with Emphasis on Active Remote Sensing (ASAR Sensor) Case study: Persepolis,Journal Of Radar and Optic Remote Sensing 2. 67–78.

Farzinkia Robabeh; Mohmmadali Zanganehasadi; Abolghasem Amirahmadi; Rahman Zandi(2019) The Relationship between Tectonic Activity and Its Impact on Land Subsidence in the Jovein Basin , Hydrogeomorphology, Volume 6, Issue 20, Pages 165-185.

Fouladi moghaddam N., Matkan A.A.,Sahebi M.R., Roustaei M (2011) Surface deformation detection by differential interferometric Sar in Aghajari Oil field, Geoscience, Volume 20, Number 80; Page(s) 103-112.

Ghadimi M, Derakhshan A.(2020) Behaviour Comparison of the Taleqan Dam Using Instrumentation Data and Radar Interferometry. Journal of Geomatics Science And Technology; 10 (2) :111-117

Ghahroudi tali, M, khadijeh alinoori (2015), Investigation of environmental changes by microlandforms in Iranian playas (Case study: Hoze Soltan playas), First International Conference on Geographical Sciences. Shiraz, Iran.ICGS2015.

Ghahroudi Tali, M., Alinoori, K., Rivandi, H. (2021). An analysis of factors affecting subsidence in Sabzevar plain. *Scientific- Research Quarterly of Geographical Data (SEPEHR)*, 30(117), 165-180. doi: 10.22131/sepehr.2021.244457

Haghighatmehr, P., Valadanzouj, M., Tajik, R., Jabari, S., Sahebi, M., Eslami, R., Ganjiyan, M., Dehghani, M. (2012). Time Series Analysis of Hashtgerd Subsidence Using Radar Interferometry and Global Positioning System. Scientific Quarterly Journal of Geosciences, 22(85), 105-114. doi: 10.22071/gsj.2012.54026

Hassanshahia Jalal & Ali Sarkargar Ardakani (2019)Quantifying Geotechnical Changes in the Rafsanjan Plain in Time Series and Finding Out Their Causes Using Radar Remote Sensing Techniques, Journal Of Radar and Optical Remote Sensing 1 71–81.

Haukos, D. A., and Smith, L. M.1994. The Importance of Playa Wetlands to Biodiversity of the Southern High Plains. Landscape and Urban Planning 28: 83-98.

Holecz F., J. Moreira, P. Pasquali, S. Voigt, E. Meier, D. Nuesch. (1997). Height Model Generation, Automatic Geocoding and Mosaicing using Airborne AeS-1 InSAR Data . Proceedings of IGARSS'97 Symposium, DOI: 10.1109/IGARSS.1997.609148.

Jafari shahin, sara atarji, mohammad ghorbani (2020) Investigation of Earth Deformation Due to Earthquake Using Radar Interference Technique,The Iranian conference on radar and surveillance systems. Malek ashtar university of technology 18-19 novamber. RADARC07_045.

karimi Omid , Seyyed Ali Almodaresi(2019) Rockfall Detection Using Differential Interference Synthetic Radar Technique from Sentinel-1 Satellite Imagery (Case study: Haraz road). Journal Of Radar and Optical Remote Sensing 1. 58–70.

Manuela Bonano, Michele Manunta, Maria Marsella & Riccardo Lanari (2012) Long-term ERS/ENVISAT deformation time-series generation at full spatial resolution via the extended SBAS technique, International Journal of Remote Sensing, 33:15, 4756-4783, DOI: 10.1080/01431161.2011.638340.

Manunta M., M. Marsella, G. Zeni, M. Sciotti, S. Atzori & R. Lanari (2008) Two- scale surface deformation analysis using the SBAS- DInSAR technique: a case study of the city of Rome, Italy, International Journal of Remote Sensing, 29:6, 1665-1684, DOI: 10.1080/01431160701395278

Pietrasiak, Nicole a., Rebecca E. Drenovsky b, Louis S. Santiago ,and Robert C.Grahama. 2014. Biogeomorphology of a Mojave Desert landscape - Configurations and feedbacks ofabiotic and biotic land surfaces during landform evolution. Geomorphology 206: 23–36.

Piri Hamed , Abolqasem Amir Ahmadi & Amed Adab (2018) Investigating the role of duality in geomorphology using radar data in Bahadoran plain of Yazd,Journal Of Radar and Optic Remote Sensing 2 .79–93.

Ramesht m.h, s,s,shahzeidi (2011) Application of Geomorphology in Regional, National, Economic planning and Tourism. Isfahan University Press.

Rosen, M. R.1994. The Importance of Groundwater in Playas: A Review of Playa Classifications and the Sedimentology and Hydrology of Playas. Paleoclimate and Basin Evolution of Playa Systems. Boulder, CO, USA, Geological Society of America 289.

Saco, P. M., Willgoose, G. R., and Hancock, G. R. . 2007. Eco-geomorphology of banded vegetation patterns in arid and semi-arid regions, Hydrol. Earth Syst. Sci., 11, 1717–1730, https://doi.org/10.5194/hess-11-1717-2007, 2007.

Schaetzl, R., and Anderson, S. 2005. Soils Genesis and Geomorphology, Cambridge, MA, USA. Cambridge University Press.

Sepehr, Adel.,and Seyed Ali Almodaresi.2013. Geotop of Lut Playa: Quaternary Geomorphologic Evidence and Civilization. Journal of Earth Science and Engineering 3: 168-179.

Shafie darabi A. et al.,(2013) Hoze sultan hunting lagoon is prohibited in Internal Report of the general office of the Environment of Qom Province. 1st ed., pp 7-49, Environment of Qom Province .

Shahram Roustaei, hasan Ahmadzadeh (2014) Radar Interferometry Techniques A New Approach to Monitoring Earth Surface Changes(Case study of landslide in Ghator region), Second National Conference on Geomorphology and Monitoring of Environmental Change. University of Tehran. 2014-03-12.

Shahram Roustaei, hasan Ahmadzadeh, mohammadreza nikju &maryam dehgani (2016) Evaluation of Site Selection for Settlements That Affected by Natural Hazards Using D-InSAR Techniques (Case Study: Googerd Village), Journal of Geography and Planning, Volume 20, Issue 55 - Serial Number 55, Pages 145-160.

Sharifikia Mohammad, Abbas Ali Afzali, Siavash Shayan (2015) Extracting and evaluating the effects of geomorphologic phenomena caused by subsidence in Damghan plain, Quantitative Geomorphological Research, 4(2), 60-74.

Shirani K, Khoshbaten M.(2016) The study and monitoring of an active landslide using differential interferometry synthetic aperture RADAR (Case study: Noghol landslide, Semirom). Quaternary journal of iran 65-53(1)2.

Smith, L. M. 2003. Playas of the Great Plains, Austin, TX, USA, University of Texas Press 257.

Stramondo. S. Corresponding author, M. Moro, F. Doumaz & F. R. Cinti (2005) The 26 December 2003, Bam, Iran earthquake: surface displacement from Envisat ASAR interferometry, International Journal of Remote Sensing, 26:5, 1027-1034, DOI: 10.1080/0143116042000295651

Tahmasebi B., A. R. Amiri-Simkooei, M. Dehghani, M. Momeni.(2015) Evaluation of Noise in Deformation Time Series Extracted by Small Baseline Interferometry. Journal of Geomatics Science And Technology. 2015; 4 (4) :83-92.

Tiner, R. W. 2003. Geographically isolated wetlands of the United States. Wetlands 3 (23): 494-516.

Wang, Lingxiao, Lin Zhao, Huayun Zhou, Shibo Liu, Erji Du, Defu Zou, Guangyue Liu, Chong Wang, and Yan Li. 2022. "Permafrost Ground Ice Melting and Deformation Time Series Revealed by Sentinel-1

InSAR in the Tanggula Mountain Region on the Tibetan Plateau" Remote Sensing 14, no. 4: 811. https://doi.org/10.3390/rs14040811

Wassie, Yismaw, S. M. Mirmazloumi, Michele Crosetto, Riccardo Palamà, Oriol Monserrat, and Bruno Crippa. 2022. "Spatio-Temporal Quality Indicators for Differential Interferometric Synthetic Aperture Radar Data" Remote Sensing 14, no. 3: 798. https://doi.org/10.3390/rs14030798